

# Transverse momentum $p_T$ spectra of strange particles production in different collisions at $\sqrt{s_{NN}} = 2.76, 5.02,$ and $7$ TeV

HAYAM YASSIN <sup>†</sup>, EMAN R. ABO ELYAZEED<sup>‡</sup>

Physics Department, Faculty of Women for Arts, Science and Education, Ain Shams University, 11577 Cairo, Egypt

We analyse the transverse momentum  $p_T$  spectra of strange particles  $K_s^0$ ,  $\Lambda$ , and  $\Xi^-$  produced in Pb+Pb collision at  $\sqrt{s_{NN}} = 2.76$  TeV, p+Pb collision at  $\sqrt{s_{NN}} = 5.02$  TeV, and p+p collision at  $\sqrt{s_{NN}} = 7$  TeV in different multiplicity events measured by the *CMS* experiment at the Large Hadron Collider. The  $p_T$  spectra of strange particles are fitted by Tsallis statistics and Boltzmann statistics, respectively. The fitting parameters are studied as a function of the multiplicity events for all systems. The Tsallis temperature ( $T_{Ts}$ ), Boltzmann temperature ( $T_{Boltz}$ ), and radius of the system ( $R$ ) increase with both the mass and strangeness number of the particle and also increase with the multiplicity events. The non-extensive parameter ( $q$ ) decreases with the increase in the mass of the particle and also decrease with the increase in the multiplicity events which means that the system tends to thermodynamic stabilization. The extracted temperatures from the two statistics for the strange particles are exhibited a linear correlation.

PACS numbers: 25.75.Dw; 25.75.-q; 24.10.Pa

## 1. Introduction

Quark-gluon plasma (QGP) was created at heavy-ion collisions at the Relativistic Heavy-Ion Collider (RHIC) and the Large Hadron Collider (LHC) [1, 2, 3]. The heavy-ion experiments seek to study strongly interacting matter under extreme conditions of high density and /or high temperatures [4]. QGP was described as the deconfinement of the colliding hadrons which rapidly expands and cools down [5]. "Hadronization" or phase transition

---

<sup>†</sup> Corresponding Author: hiam\_hussien@women.asu.edu.eg

<sup>‡</sup> eman.reda@women.asu.edu.eg

from QGP to hadrons found at the combination of the quarks and gluons at special temperatures defined as critical temperatures. After cooling again, chemical freeze-out occur where the produced particles are stable [6]. One of the signatures for the creation of QGP is the enhancement of the strangeness number [7, 8]. Strange quarks are not produced into the reaction by the colliding nuclei. Therefore, any strange quarks or anti-quarks seen in experiments have been newly created from the kinetic energy of the colliding nuclei [8, 9]. Also, another important indication for the formation of QGP is the transverse momentum  $p_T$  spectra of the charged and strange particles [10]. Because the  $p_T$  spectra can give information about the chemical freezeout - chemical potential and temperature - by utilizing many statistical models [11, 12, 13, 14, 15, 16, 17]. These statistical models describe the experimental measurements over a wide range of center-of-mass energies depending on different statistics.

Tsallis statistics [18, 19, 20, 21, 22, 23] success in fitting the experimental data [24, 25] of the transverse momentum  $p_T$  spectra in high energy physics. The  $p_T$  spectra of all identified particles which measured in p+p collisions at RHIC and LHC energies was fitted excellently by Tsallis statistics in Ref. [26, 27, 28]. The Tsallis statistics with the transverse flow effect is used in the analysis of the  $p_T$  spectra of charged and strange particles in Ref. [29, 30, 31, 22, 23, 32]. Tsallis and Boltzmann statistics describe the  $p_T$  spectra of all identified particles measured in Au+Au collision and Pb+Pb collision at RHIC and LHC energies in Ref. [33]. Also, the obtained temperatures from these previous fitting gave some useful correlations with each other. The aim of this paper is to obtain the correlation between the Tsallis and Boltzmann temperatures from the  $p_T$  spectra of strange particles at different collisions and energies.

The paper is organized as follows. In Sect. 2.1, the Tsallis statistics is presented, which is used to describe the particle spectra. In Sect. 2.2, we present the Boltzmann statistics which is used to describe the particle spectra. Then we discuss the results of the description of the  $p_T$  spectra of strange particles at different collisions and energies by using both statistics in Sect. 3. Also, the dependence of the fitting parameters on the multiplicity events and particle mass is discussed in Sect. 3. Finally, in Sect. 4 the conclusion of our results is presented.

## 2. Transverse momentum spectra

Transverse momentum  $p_T$  spectra of strange particles  $K_s^0$ ,  $\Lambda$ , and  $\Xi^-$  produced in Pb+Pb collision at  $\sqrt{s_{NN}} = 2.76$  TeV, p+Pb collision at  $\sqrt{s_{NN}} = 5.02$  TeV, and p+p collision at  $\sqrt{s_{NN}} = 7$  TeV which measured by the *CMS* experiment will be discussed using Tsallis and Boltzmann statistics in the

following Sects. 2.1 and 2.2.

### 2.1. Tsallis statistics

The experimental measurements of the  $p_T$  spectra in high-energy collisions can be described by different formula of Tsallis statistics [18, 34, 35, 36]. The total number of particles is given by

$$N = \frac{gV}{(2\pi)^3} \int_0^\infty \left[ 1 + (q-1) \left( \frac{E-\mu}{T_{Ts}} \right) \right]^{\frac{q}{1-q}} dp^3, \quad (1)$$

where,  $T_{Ts}$  is the Tsallis temperature,  $q$  is the non-extensive parameter,  $E$  is the energy,  $p$  is the pressure,  $g$  is the degeneracy factor,  $V$  is the system volume, and  $\mu$  is the chemical potential. The momentum distribution [37] can be obtained as

$$E \frac{d^3N}{dp^3} = \frac{gVE}{(2\pi)^3} \left[ 1 + (q-1) \left( \frac{E-\mu}{T_{Ts}} \right) \right]^{\frac{q}{1-q}}. \quad (2)$$

In terms of the rapidity ( $y$ ) and the transverse mass ( $m_T = \sqrt{p_T^2 + m^2}$ ), energy can be written as  $E = m_T \cosh y$ , so at mid-rapidity  $y = 0$  and  $\mu \approx 0$ , Eq. 2 [38] becomes

$$\frac{1}{2\pi p_T} \frac{d^2N}{dp_T dy} \Big|_{y=0} = \frac{gVm_T}{(2\pi)^3} \left[ 1 + (q-1) \left( \frac{m_T}{T_{Ts}} \right) \right]^{\frac{q}{1-q}}. \quad (3)$$

### 2.2. Boltzmann statistics

According to Boltzmann statistics [39], the number of particles can be written as

$$N = \frac{gV}{(2\pi)^3} \int_0^\infty \frac{dp^3}{\exp\left(\frac{E-\mu}{T_{Boltz}}\right)}, \quad (4)$$

where  $T_{Boltz}$  is the Boltzmann temperature. The momentum distribution [39, 40, 41] can be obtained as

$$E \frac{d^3N}{dp^3} = \frac{gVE}{(2\pi)^3} \exp\left(\frac{\mu-E}{T_{Boltz}}\right). \quad (5)$$

The momentum distribution at mid-rapidity  $y = 0$  and  $\mu \approx 0$  can be given by

$$\frac{1}{2\pi p_T} \frac{d^2N}{dp_T dy} \Big|_{y=0} = \frac{gVm_T}{(2\pi)^3} \exp\left(-\frac{m_T}{T_{Boltz}}\right). \quad (6)$$

### 3. Results and Discussion

The transverse momentum distributions of the strange particles  $K_s^0$ ,  $\Lambda$ , and  $\Xi^-$  in Pb+Pb collision at  $\sqrt{s_{NN}} = 2.76$  TeV, p+Pb collision at  $\sqrt{s_{NN}} = 5.02$  TeV, and p+p collision at  $\sqrt{s_{NN}} = 7$  TeV [42] in different multiplicity intervals are fitted using two different kinds of statistics. Boltzmann statistics using Eq. 6 and Tsallis statistics using Eq. 3. These are shown in Figs. 1, 2, and 3. The fitting parameters are listed in Tables 1, 2, and 3.

Figure 1 shows the  $p_T$  spectra of the strange particles, (a)  $K_s^0$ , (b)  $\Lambda$ , and (c)  $\Xi^-$ , produced in Pb+Pb collision at  $\sqrt{s_{NN}} = 2.76$  TeV with different multiplicity intervals. The experimental data of the *CMS* experiment [42] are represented by symbols. The experimental data are divided into classes based on the multiplicity intervals  $N_{\text{trk}}^{\text{offline}}$  in the mid-rapidity range  $|y| < 1.0$ . The corresponding averaged multiplicity  $\langle N_{\text{track}} \rangle = 21, 58, 92, 130, 168, 210, 253$  and 299 [43]. The solid and dashed curves are the calculated results using the Tsallis statistics (Eq. 3) and the Boltzmann statistics (Eq. 6), respectively. Here, we concentrate on the smallest  $p_T$  region. The resulting fit parameters are given in Table 1. We notice that our two results for  $\Lambda$  and  $\Xi^-$  particles are in good agreement with the experimental data of Pb+Pb collisions at  $\sqrt{s_{NN}} = 2.76$  TeV for all multiplicity intervals. For  $K_s^0$  particle, also there is a good agreement only with the results obtained from Tsallis statistics but with the results obtained from Boltzmann statistics, the good agreement decreases with the increase in the multiplicity classes.

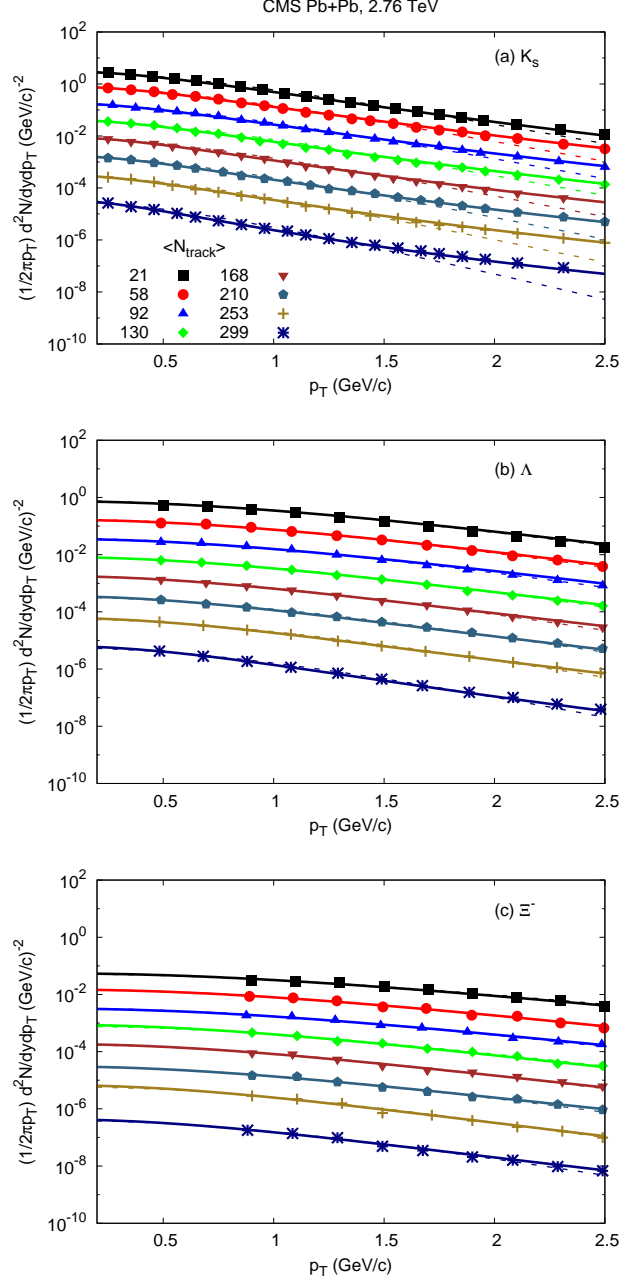


Fig. 1: (Color online) Transverse momentum distributions of the strange particles  $K_s^0$ ,  $\Lambda$ , and  $\Xi^-$  for Pb+Pb collision at  $\sqrt{s_{NN}} = 2.76$  TeV measured in *CMS* [42] experiment (symbols) are compared with calculations from Tsallis statistics (solid curves) using Eq. 3 and with Boltzmann statistics (dashed curves) using Eq. 6 for different multiplicity intervals.

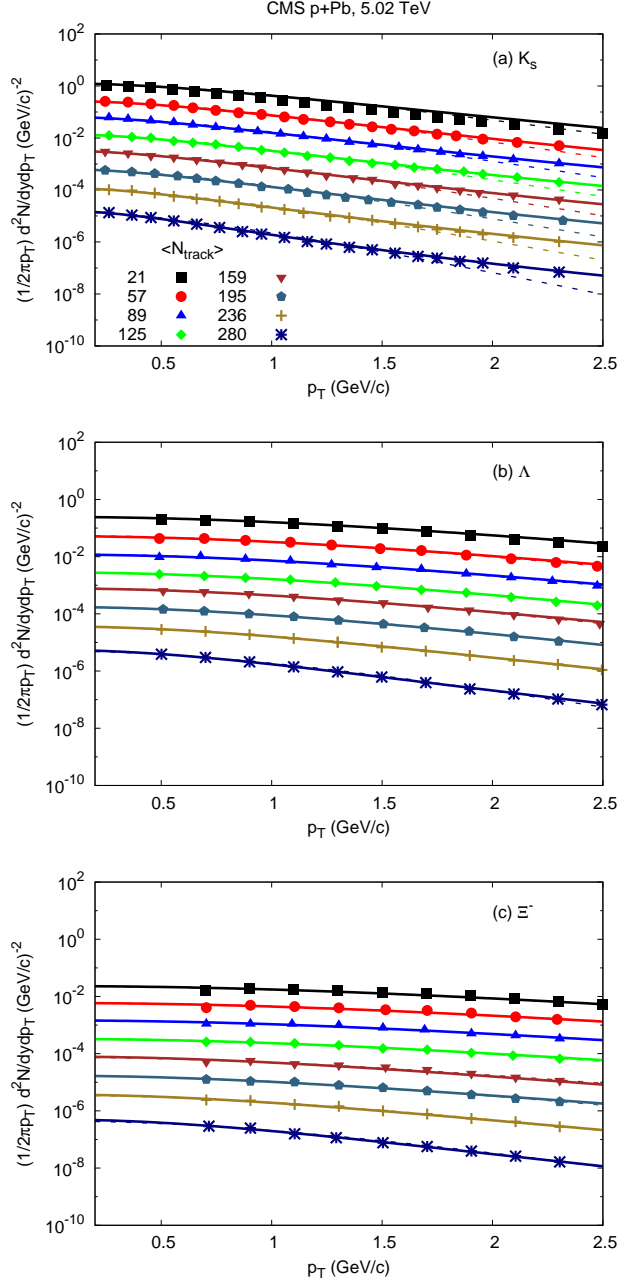


Fig. 2: (Color online) Transverse momentum distributions of the strange particles  $K_s^0$ ,  $\Lambda$ , and  $\Xi^-$  for p+Pb collision at  $\sqrt{s_{NN}} = 5.02$  TeV measured in *CMS* [42] experiment (symbols) are compared with calculations from Tsallis statistics (solid curves) using Eq. 3 and with Boltzmann statistics (dashed curves) using Eq. 6 for different multiplicity intervals.

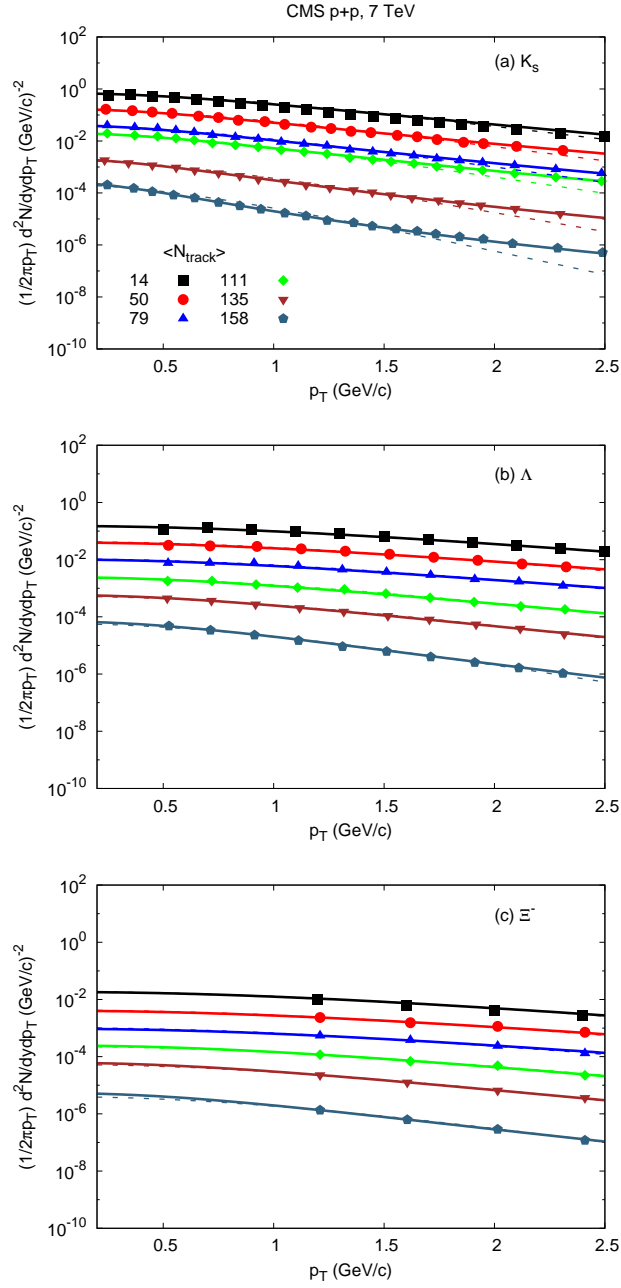


Fig. 3: (Color online) Transverse momentum distributions of the strange particles  $K_s^0$ ,  $\Lambda$ , and  $\Xi^-$  for p+p collision at  $\sqrt{s_{NN}} = 7$  TeV measured in *CMS* [42] experiment (symbols) are compared with calculations from Tsallis statistics (solid curves) using Eq. 3 and with Boltzmann statistics (dashed curves) using Eq. 6 for different multiplicity intervals.

Table 1: Parameters deduced for the fitting of Tsallis and Boltzmann transverse momentum distributions at different multiplicity intervals for Pb+Pb collision at  $\sqrt{s_{NN}} = 2.76$  TeV, Fig. 1.

Particle	$\langle N_{\text{track}} \rangle$	$T_{\text{Ts}}$ [MeV]	$q$	$R$ [fm]	$\chi^2/\text{dof}$	$T_{\text{Boltz}}$ [MeV]	$R$ [fm]	$\chi^2/\text{dof}$
$K_s^0$	21	$87.169 \pm 0.105$	$1.15 \pm 0.001$	$0.154 \pm 0.026$	0.023	$198.808 \pm 1.672$	$0.07 \pm 0.021$	0.13
	58	$133.113 \pm 0.378$	$1.1224 \pm 0.003$	$0.211 \pm 0.044$	0.047	$220.873 \pm 1.47$	$0.136 \pm 0.036$	0.1
	92	$139.857 \pm 0.131$	$1.1189 \pm 0.001$	$0.358 \pm 0.052$	0.015	$228.78 \pm 1.46$	$0.236 \pm 0.062$	0.09
	130	$147.611 \pm 0.283$	$1.1158 \pm 0.002$	$0.589 \pm 0.107$	0.03	$238.526 \pm 1.749$	$0.394 \pm 0.107$	0.1
	168	$165.663 \pm 0.418$	$1.1017 \pm 0.003$	$0.894 \pm 0.175$	0.038	$248.365 \pm 1.7$	$0.642 \pm 0.169$	0.091
	210	$170.876 \pm 0.345$	$1.1007 \pm 0.003$	$1.421 \pm 0.257$	0.03	$248.671 \pm 1.624$	$1.051 \pm 0.273$	0.087
	253	$181.643 \pm 0.294$	$1.0941 \pm 0.002$	$2.226 \pm 0.371$	0.023	$249.084 \pm 1.053$	$1.741 \pm 0.391$	0.056
	299	$188.54 \pm 0.499$	$1.079 \pm 0.004$	$3.381 \pm 0.622$	0.031	$256.769 \pm 2.215$	$2.65 \pm 0.737$	0.108
$\Lambda$	21	$91.274 \pm 0.084$	$1.11 \pm 0.0003$	$0.193 \pm 0.034$	0.056	$249.745 \pm 1.111$	$0.046 \pm 0.013$	0.233
	58	$160.973 \pm 0.093$	$1.09 \pm 0.0003$	$0.166 \pm 0.024$	0.03	$289.72 \pm 0.944$	$0.082 \pm 0.02$	0.15
	92	$187.226 \pm 0.27$	$1.08 \pm 0.001$	$0.242 \pm 0.046$	0.07	$304.703 \pm 1.244$	$0.137 \pm 0.036$	0.181
	130	$229.993 \pm 0.164$	$1.064 \pm 0.001$	$0.321 \pm 0.047$	0.032	$309.954 \pm 0.359$	$0.235 \pm 0.04$	0.05
	168	$274.28 \pm 0.412$	$1.0429 \pm 0.001$	$0.441 \pm 0.082$	0.064	$329.929 \pm 0.511$	$0.366 \pm 0.068$	0.064
	210	$322.756 \pm 1.085$	$1.0245 \pm 0.003$	$0.605 \pm 0.143$	0.132	$335.32 \pm 1.454$	$0.597 \pm 0.156$	0.178
	253	$343.331 \pm 1.146$	$1.0086 \pm 0.003$	$0.957 \pm 0.179$	0.13	$340.261 \pm 1.479$	$0.982 \pm 0.255$	0.176
	299	$362.632 \pm 0.633$	$1.0067 \pm 0.002$	$1.488 \pm 0.279$	0.066	$360.228 \pm 0.887$	$1.515 \pm 0.321$	0.095
$\Xi^-$	21	$156.108 \pm 0.513$	$1.09 \pm 0.001$	$0.042 \pm 0.011$	0.246	$290.041 \pm 1.119$	$0.019 \pm 0.165$	0.284
	58	$188.975 \pm 0.719$	$1.07 \pm 0.001$	$0.081 \pm 0.023$	0.282	$309.878 \pm 1.633$	$0.042 \pm 0.12$	0.367
	92	$257.487 \pm 1.258$	$1.0599 \pm 0.003$	$0.085 \pm 0.025$	0.312	$340.112 \pm 2.124$	$0.063 \pm 0.075$	0.402
	130	$265.875 \pm 1.243$	$1.052 \pm 0.002$	$0.151 \pm 0.043$	0.3	$349.961 \pm 2.211$	$0.11 \pm 0.047$	0.394
	168	$286.238 \pm 0.784$	$1.0441 \pm 0.002$	$0.231 \pm 0.055$	0.172	$379.967 \pm 1.907$	$0.164 \pm 0.035$	0.292
	210	$365.428 \pm 1.569$	$1.0248 \pm 0.003$	$0.27 \pm 0.072$	0.238	$390.23 \pm 2.162$	$0.257 \pm 0.02$	0.314
	253	$377.162 \pm 1.579$	$1.0168 \pm 0.003$	$0.437 \pm 0.116$	0.232	$400.073 \pm 2.165$	$0.414 \pm 0.013$	0.301
	299	$425.295 \pm 2.719$	$1.0152 \pm 0.005$	$0.595 \pm 0.176$	0.322	$470.406 \pm 3.561$	$0.533 \pm 0.005$	0.368



Table 2: Parameters deduced for the fitting of Tsallis and Boltzmann transverse momentum distributions at different multiplicity intervals for p+Pb collision collision at  $\sqrt{s_{NN}} = 5.02$  TeV, Fig. 2.

Particle	$\langle N_{\text{track}} \rangle$	$T_{\text{Ts}}$ [MeV]	$q$	$R$ [fm]	$\chi^2/\text{dof}$	$T_{\text{Boltz}}$ [MeV]	$R$ [fm]	$\chi^2/\text{dof}$
$K_s^0$	21	$133.898 \pm 0.295$	$1.1307 \pm 0.002$	$0.077 \pm 0.015$	0.035	$228.653 \pm 1.589$	$0.049 \pm 0.013$	0.098
	57	$179.121 \pm 0.646$	$1.1147 \pm 0.005$	$0.118 \pm 0.026$	0.051	$256.887 \pm 1.525$	$0.09 \pm 0.023$	0.078
	89	$199.756 \pm 0.687$	$1.1083 \pm 0.005$	$0.19 \pm 0.04$	0.046	$269.206 \pm 1.133$	$0.153 \pm 0.034$	0.054
	125	$206.332 \pm 0.489$	$1.1047 \pm 0.004$	$0.32 \pm 0.059$	0.031	$278.893 \pm 1.433$	$0.258 \pm 0.06$	0.064
	159	$218.697 \pm 0.833$	$1.1021 \pm 0.006$	$0.497 \pm 0.106$	0.048	$288.99 \pm 1.548$	$0.409 \pm 0.096$	0.065
	195	$226.848 \pm 1.085$	$1.1005 \pm 0.008$	$0.81 \pm 0.185$	0.06	$294.12 \pm 1.769$	$0.678 \pm 0.165$	0.072
	236	$255.94 \pm 1.87$	$1.0787 \pm 0.013$	$1.205 \pm 0.312$	0.087	$309.36 \pm 2.499$	$1.063 \pm 0.282$	0.093
	280	$293.332 \pm 1.425$	$1.0676 \pm 0.009$	$1.869 \pm 0.419$	0.056	$334.762 \pm 1.591$	$1.721 \pm 0.382$	0.055
$\Lambda$	21	$172.072 \pm 0.124$	$1.09 \pm 0.0004$	$0.067 \pm 0.01$	0.036	$299.715 \pm 0.865$	$0.035 \pm 0.008$	0.13
	57	$297.482 \pm 0.386$	$1.0499 \pm 0.001$	$0.065 \pm 0.011$	0.052	$369.708 \pm 0.797$	$0.053 \pm 0.011$	0.083
	89	$373.144 \pm 0.253$	$1.0249 \pm 0.001$	$0.089 \pm 0.012$	0.024	$409.837 \pm 0.47$	$0.082 \pm 0.013$	0.04
	125	$436.177 \pm 1.142$	$1.0091 \pm 0.003$	$0.127 \pm 0.026$	0.085	$430.532 \pm 1.625$	$0.131 \pm 0.031$	0.127
	159	$453.51 \pm 0.919$	$1.0065 \pm 0.003$	$0.19 \pm 0.035$	0.064	$460.097 \pm 1.122$	$0.188 \pm 0.037$	0.077
	195	$482.8 \pm 2.922$	$1.0047 \pm 0.008$	$0.292 \pm 0.077$	0.183	$470.728 \pm 3.661$	$0.302 \pm 0.087$	0.243
	236	$501.749 \pm 2.302$	$1.0034 \pm 0.007$	$0.465 \pm 0.111$	0.135	$480.908 \pm 2.991$	$0.487 \pm 0.13$	0.192
	280	$531.914 \pm 2.423$	$1.0012 \pm 0.007$	$0.747 \pm 0.176$	0.131	$535.578 \pm 2.905$	$0.744 \pm 0.186$	0.157
$\Xi^-$	21	$192.967 \pm 0.508$	$1.083 \pm 0.001$	$0.031 \pm 0.008$	0.176	$339.7 \pm 1.556$	$0.016 \pm 0.009$	0.277
	57	$301.869 \pm 1.753$	$1.0711 \pm 0.004$	$0.034 \pm 0.01$	0.306	$420.171 \pm 1.799$	$0.024 \pm 0.006$	0.217
	89	$396.942 \pm 2.066$	$1.0684 \pm 0.005$	$0.042 \pm 0.011$	0.232	$480.405 \pm 2.054$	$0.036 \pm 0.019$	0.194
	125	$423.094 \pm 4.797$	$1.049 \pm 0.013$	$0.067 \pm 0.023$	0.547	$531.027 \pm 4.793$	$0.054 \pm 0.017$	0.38
	159	$568.425 \pm 26.71$	$1.0287 \pm 0.01$	$0.084 \pm 0.022$	0.236	$580.505 \pm 3.308$	$0.083 \pm 0.022$	0.222
	195	$610.815 \pm 6.597$	$1.0219 \pm 0.02$	$0.131 \pm 0.041$	0.382	$630.846 \pm 6.12$	$0.128 \pm 0.039$	0.317
	236	$642.08 \pm 7.933$	$1.0189 \pm 0.019$	$0.202 \pm 0.066$	0.437	$662.482 \pm 9.601$	$0.198 \pm 0.069$	0.051
	280	$660.022 \pm 10.78$	$1.0139 \pm 0.04$	$0.311 \pm 0.111$	0.558	$672.726 \pm 9.541$	$0.308 \pm 0.104$	0.488

TsallisBoltzmannA CPB printed on December 18, 2018

Figure 2 represents the  $p_T$  spectra of the strange particles, (a)  $K_s^0$ , (b)  $\Lambda$ , and (c)  $\Xi^-$ , produced in p+Pb collisions at  $\sqrt{s_{NN}} = 5.02$  TeV with different multiplicity intervals. The experimental data of the *CMS* experiment [42] are represented by symbols. The experimental data are divided into classes based on the multiplicity intervals  $N_{\text{trk}}^{\text{offline}}$  in the mid-rapidity range  $|y| < 1.0$ . The corresponding averaged multiplicity  $\langle N_{\text{trk}} \rangle = 21, 57, 89, 125, 159, 195, 236$  and 280 [43]. The solid and dashed curves are the calculated results using the Tsallis statistics (Eq. 3) and the Boltzmann statistics (Eq. 6), respectively. Here, we concentrate on the smallest  $p_T$  region. The resulting fit parameters are given in Table 2. We notice that our two results for  $\Lambda$  and  $\Xi^-$  particles are in good agreement with the experimental data of p+Pb collisions at  $\sqrt{s_{NN}} = 5.02$  TeV for all multiplicity intervals. For  $K_s^0$  particle, also there is a good agreement only with the results obtained from Tsallis statistics but with the results obtained from Boltzmann statistics, the good agreement decrease with the increasing of the multiplicity classes.

Figure 3 depicts the  $p_T$  spectra of the strange particles, (a)  $K_s^0$ , (b)  $\Lambda$ , and (c)  $\Xi^-$ , produced in p+p collision at  $\sqrt{s_{NN}} = 7$  TeV with different multiplicity intervals. The experimental data of the *CMS* experiment [42] are represented by symbols. The experimental data are divided into classes based on the multiplicity intervals  $N_{\text{trk}}^{\text{offline}}$  in the mid-rapidity range  $|y| < 1.0$ . The corresponding averaged multiplicity  $\langle N_{\text{trk}} \rangle = 14, 50, 79, 111, 135$  and 158 [43]. The solid and dashed curves are the calculated results using the Tsallis statistics (Eq. 3) and the Boltzmann statistics (Eq. 6), respectively. Here, we concentrate on the smallest  $p_T$  region. The resulting fit parameters are given in Table 3. We notice that our two results for  $\Lambda$  and  $\Xi^-$  particles are in good agreement with the experimental data of p+p collisions at  $\sqrt{s_{NN}} = 7$  TeV for all multiplicity intervals. For  $K_s^0$  particle, also there is a good agreement only with the results obtained from Tsallis statistics but with the results obtained from Boltzmann statistics, the good agreement decrease with the increase in the multiplicity intervals.

As seen from Tables 1, 2, and 3, the value of  $\chi^2/\text{dof}$  is so small which represents the good quality of the fitting. Especially, the Tsallis statistics that gives excellent agreement with the experimental measurements for all multiplicity classes. Also, the fitting results by Tsallis statistics are better than those of Boltzmann statistics, especially at high range of  $p_T$ .

Furthermore, we have extracted the fitting parameters the non-extensive parameter  $q$ , the Tsallis temperature parameter  $T_{\text{Ts}}$ , and the Boltzmann temperature parameter  $T_{\text{Boltz}}$  which inform us about the variations between Tsallis statistics and Boltzmann statistics. Also, there is another fitting parameter known as the radius  $R$  as we assume the geometry of the fireball is spherical so  $R = (3V/4\pi)^{1/3}$  which signifies the dimension of the system

and is related to the normalization in the statistical distribution function which used in describing the particle yield or spectra [44].

Figure 4 (a-c) depict the fitting parameter  $q$  for the strange particles  $K_s^0$ ,  $\Lambda$ , and  $\Xi^-$  as a function of  $\langle N_{\text{track}} \rangle$  produced in the Pb+Pb, p+Pb, and p+p collisions at  $\sqrt{s_{\text{NN}}} = 2.76, 5.02$ , and 7 TeV, respectively. Results are obtained using Tsallis statistics and modified Tsallis statistics [30]. The value of  $q$  (our calculations) decreases with the increasing of both the particle mass and strangeness number and also with the increasing in the multiplicity events for all systems. Our results different from modified one in the effect of multiplicity on the non-extensivity parameter. This decreasing indicate that the system tend to be in equilibrium (thermodynamically).

Figure 5 (a-c) show the fitting parameter  $R$  for the strange particles  $K_s^0$ ,  $\Lambda$ , and  $\Xi^-$  as a function of  $\langle N_{\text{track}} \rangle$  produced in the Pb+Pb, p+Pb, and p+p collisions at  $\sqrt{s_{\text{NN}}} = 2.76, 5.02$ , and 7 TeV, respectively. The value of  $R$  increases with the increasing in the multiplicity classes but decreases with the increase in the particle mass. So the volume of the system increases with the increase in the multiplicity events as expected.

We compare our obtained values of  $R$  with Hanbury-BrownTwiss (HBT) radii [45, 46, 47] at different center-of-mass energies  $\sqrt{s_{\text{NN}}}$  as shown in Fig. 6. The fitting parameter  $R$  for the strange particles  $K_s^0$ ,  $\Lambda$ , and  $\Xi^-$  and from HBT radii obtained at most central collisions and also at mid-rapidity (for details on HBT radius parameters, see Refs. [48, 49, 50, 51, 52]). The obtained values of  $R$  were in the same behaviour as  $R$  from HBT especially  $R_{\text{long}}$ .

Figure 7 (a-c) depict the fitting parameter  $T$  for the strange particles  $K_s^0$ ,  $\Lambda$ , and  $\Xi^-$  as a function of  $\langle N_{\text{track}} \rangle$  produced in the Pb+Pb, p+Pb, and p+p collisions at  $\sqrt{s_{\text{NN}}} = 2.76, 5.02$ , and 7 TeV, respectively. The value of both temperatures (Tsallis and Boltzmann) increase with the increasing in both the particle mass and the strangeness number and also with the multiplicity classes for all systems. The direct relationship between the temperature and the strangeness number of hadrons is unlike the known behaviour obtained previously in extensive models (particle yields and ratios) [53, 54], so we will work on the confirmation of the behaviour of this dependence in extensive and nonextensive particle yields and ratios in future work. Our calculations are compared with the modified Tsallis results [30] and agreed with each other. The freeze-out of particles with large mass occur earlier than that of small mass. When volume is small, the particle with large mass freeze-out early [4]. Also, the Boltzmann temperature always greater than the Tsallis one which are independent on the type of particles or systems so  $T_{\text{Boltz}} > T_{\text{Ts}}$ .

Table 3: Parameters deduced for the fitting of Tsallis and Boltzmann transverse momentum distributions at different multiplicity intervals for p+p collision at  $\sqrt{s_{NN}} = 7$  TeV, Fig. 3.

Particle	$\langle N_{\text{track}} \rangle$	$T_{\text{Ts}}$ [MeV]	$q$	$R$ [fm]	$\chi^2/\text{dof}$	$T_{\text{Boltz}}$ [MeV]	$R$ [fm]	$\chi^2/\text{dof}$
$K_s^0$	14	$91.407 \pm 0.129$	$1.154 \pm 0.001$	$0.282 \pm 0.049$	0.026	$213.472 \pm 2.176$	$0.126 \pm 0.04$	0.159
	50	$155.351 \pm 0.397$	$1.1328 \pm 0.003$	$0.337 \pm 0.066$	0.037	$258.135 \pm 2.336$	$0.225 \pm 0.065$	0.123
	79	$234.716 \pm 1.78$	$1.1047 \pm 0.013$	$0.536 \pm 0.142$	0.093	$294.827 \pm 2.402$	$0.463 \pm 0.125$	0.097
	111	$235.749 \pm 1.784$	$1.1028 \pm 0.013$	$0.673 \pm 0.178$	0.093	$308.689 \pm 2.798$	$0.561 \pm 0.155$	0.105
	135	$252.973 \pm 1.445$	$1.1082 \pm 0.011$	$1.042 \pm 0.247$	0.067	$333.049 \pm 2.631$	$0.869 \pm 0.226$	0.088
	158	$313.052 \pm 1.92$	$1.0691 \pm 0.011$	$1.472 \pm 0.355$	0.07	$359.903 \pm 2.047$	$1.355 \pm 0.317$	0.064
$\Lambda$	14	$152.631 \pm 0.284$	$1.0945 \pm 0.0008$	$0.183 \pm 0.039$	0.094	$289.682 \pm 1.218$	$0.082 \pm 0.023$	0.209
	50	$259.374 \pm 0.211$	$1.08 \pm 0.001$	$0.186 \pm 0.028$	0.033	$379.636 \pm 1.303$	$0.127 \pm 0.03$	0.136
	79	$321.4 \pm 1.805$	$1.0714 \pm 0.005$	$0.241 \pm 0.066$	0.202	$419.733 \pm 2.041$	$0.193 \pm 0.05$	0.178
	111	$413.873 \pm 3.627$	$1.0688 \pm 0.011$	$0.309 \pm 0.093$	0.268	$490.01 \pm 3.286$	$0.278 \pm 0.077$	0.216
	135	$459.049 \pm 2.757$	$1.0519 \pm 0.008$	$0.452 \pm 0.118$	0.176	$500.921 \pm 2.72$	$0.434 \pm 0.113$	0.175
	158	$501.352 \pm 3.193$	$1.0336 \pm 0.009$	$0.661 \pm 0.173$	0.18	$541.774 \pm 4.08$	$0.627 \pm 0.174$	0.213
$\Xi^-$	14	$155.92 \pm 0.093$	$1.099 \pm 0.0002$	$0.093 \pm 0.014$	0.045	$339.888 \pm 0.995$	$0.032 \pm 0.008$	0.203
	50	$274.655 \pm 0.151$	$1.076 \pm 0.0003$	$0.096 \pm 0.013$	0.034	$409.925 \pm 1.02$	$0.062 \pm 0.014$	0.146
	79	$419.894 \pm 1.824$	$1.0299 \pm 0.003$	$0.098 \pm 0.026$	0.229	$489.854 \pm 3.369$	$0.084 \pm 0.025$	0.345
	111	$516.464 \pm 1.844$	$1.028 \pm 0.004$	$0.128 \pm 0.03$	0.159	$520.321 \pm 2.446$	$0.131 \pm 0.034$	0.225
	135	$528.961 \pm 2.024$	$1.027 \pm 0.004$	$0.204 \pm 0.048$	0.164	$540.85 \pm 4.672$	$0.205 \pm 0.065$	0.403
	158	$539.162 \pm 3.965$	$1.0204 \pm 0.008$	$0.333 \pm 0.099$	0.326	$554.286 \pm 5.984$	$0.329 \pm 0.111$	0.485

Table 4: Constants values deduced from the fitting of linear relation between Tsallis and Boltzmann temperatures, Fig. 8.

Particle	$a$	$b$	$\chi^2/\text{dof}$
$K_s^0$	$(1.3714 \pm 0.0092)$	$(-177.514 \pm 2.503)$	0.0319
$\Lambda$	$(1.3856 \pm 0.0255)$	$(-209.84 \pm 10.2)$	0.0876
$\Xi^-$	$(1.39513 \pm 0.0212)$	$(-249.213 \pm 9.963)$	0.0722

Fig. 8 shows the relation between  $T_{\text{Ts}}$  and  $T_{\text{Boltz}}$ , where all values of temperatures obtained from Figs. 1, 2, and 3 which listed in Tables 1, 2, and 3 are given by symbols. The fitted result for all strange particles at different collisions is given by the solid line which is described by

$$T_{\text{Ts}} = a T_{\text{Boltz}} + b,$$

where  $a = 1.2465 \pm 0.0138$  and  $b = -160.499 \pm 5.386$  are constants with  $\chi^2/\text{dof} = 0.0528$ . But these values are different for different particles. So this linear relations is the same for all particles but the value of constants different depending on the mass of the particle. The dependence of the constants on the particle type is listed in Table 4.

As can be seen from Table 4, the value of constant  $a$  increase with the increasing of the particle mass but constant  $b$  inversely proportional to the particle mass. A similar linear relation between  $T_{\text{Ts}}$  and  $T_{\text{Boltz}}$  for charged (but not strange) particles at various collisions was found in Ref. [33]. The values of constants  $a$  and  $b$  for the charged non-strange particles confirm our concept about the dependence of the constants on the particle mass.

Therefore, we can find a direct relation between any temperature and Boltzmann temperature and considering Boltzmann temperature as the "reference" for all other temperatures [33]. However, Boltzmann statistics fails to fit some experimental transverse momentum spectra especially at high  $p_{\text{T}}$  region as a result of using the simplest form of Boltzmann statistics [16, 41, 55, 33]. On the contrary, Tsallis statistics succeeded in depicting all experimental transverse momentum spectra used in the present work and also at high region of  $p_{\text{T}}$  [30, 33, 35, 56, 57, 58, 59, 60, 61]. We also compare our Tsallis results with modified Tsallis one [30] (with a radial flow). Our Tsallis temperatures are greater than modified one [30]. The reason for this increasing gets from neglecting the effect of the radial flow. We neglect this parameter as a result of the considered low range of transverse momentum [33].

#### 4. Conclusion

We analysed the transverse momentum  $p_T$  spectra of the strange particles  $K_s^0$ ,  $\Lambda$ , and  $\Xi^-$  in different multiplicity events produced in Pb+Pb collision at  $\sqrt{s_{NN}} = 2.76$  TeV, p+Pb collision at  $\sqrt{s_{NN}} = 5.02$  TeV, and p+p collision at  $\sqrt{s_{NN}} = 7$  TeV using Tsallis and Boltzmann statistics. In all cases nearly, our Tsallis and Boltzmann results are in excellent agreement with the experimental data of *CMS* collaboration at the LHC. Except for  $K_s^0$ , the goodness of our Boltzmann result decreases with the increase in the multiplicity events.

In all studied collisions, for all particles in different multiplicity events, the Tsallis  $T_{Ts}$  and Boltzmann  $T_{Boltz}$  temperatures values increase with the increasing in the mass of the mentioned particle. Also, there is a direct relationship between the values of the temperatures and the multiplicity events. We observe that  $T_{Ts} < T_{Boltz}$ , the value of  $q$  is proportional inversely with the multiplicity events in all studied systems, and the value of  $R$  in both statistics increases with the increase in the multiplicity events. As the direct dependence of the multiplicity on the size of the volume of the system.

There is a linear relation between the Tsallis temperature  $T_{Ts}$  and the Boltzmann temperature  $T_{Boltz}$ . We have  $T_{Ts} = (1.3714 \pm 0.0092) T_{Boltz} + (-177.514 \pm 2.503)$  for  $K_s^0$ ,  $T_{Ts} = (1.3856 \pm 0.0255) T_{Boltz} + (-209.84 \pm 10.2)$  for  $\Lambda$ , and  $T_{Ts} = (1.39513 \pm 0.0212) T_{Boltz} + (-249.213 \pm 9.963)$  for  $\Xi^-$ . Also, we have  $T_{Ts} = (1.2465 \pm 0.0138) T_{Boltz} + (-160.499 \pm 5.386)$  for all studied strange particles. In all cases,  $T_{Ts} < T_{Boltz}$  as the Boltzmann temperature is considered as the base for all other temperatures, and both values of temperatures increase with the increasing in the particle mass at vanishing chemical potential.

#### REFERENCES

- [1] J.D. Bjorken, Phys. Rev. D **27**, 140 (1983).
- [2] T. Ullrich, B. Wyslouch, J.W. Harris, Nucl. Phys. A **904-905**, 1c (2013).
- [3] M. Gyulassy, L. McLerran, Nucl. Phys. A **750**, 30 (2005).
- [4] A. Khuntia, S. Tripathy, R. Sahoo, J. Cleymans, Eur. Phys. J. A **53**, 103 (2017).
- [5] S. Ahmad, A. Ahmad, A. Chandra, M. Zafar, M. Irfan, Adv. High Energy Phys. **2013**, 836071 (2013).
- [6] A. Tawfik, Int. J. Mod. Phys. A **29**, 1430021 (2014).
- [7] J. Letessier, J. Rafelski, A. Tounsi, Phys. Rev. C **50**, 406 (1994).
- [8] J. Adam et al. (ALICE collaboration), Nature Phys. **13**, 535 (2017).

- [9] J. Rafelski, B. Muller, Phys. Rev. Lett. **48**, 1066 (1982). Erratum: Phys. Rev. Lett. **56**, 2334 (1986).
- [10] H-C Song, S.A. Bass, U.W. Heinz, T. Hirano, C. Shen, Phys. Rev. Lett. **106**, 192301 (2011), Erratum: Phys. Rev. Lett. **109**, 139904 (2012).
- [11] J. Adams et al. (STAR Collaboration), Phys. Rev. Lett. **92**, 112301 (2004).
- [12] F. Becattini, J. Phys. Conf. Ser. **5**, 175 (2005).
- [13] A.H. Mueller, Nucl. Phys. B **415**, 373 (1994).
- [14] A.H. Mueller, B. Patel, Nucl. Phys. B **425**, 471 (1994).
- [15] A.H. Mueller, Nucl. Phys. B **437**, 107 (1995).
- [16] E. Schnedermann, J. Sollfrank, U.W. Heinz, Phys. Rev. C **48**, 2462 (1993).
- [17] A.N. Tawfik, H. Yassin, E.R. Abo Elyazeed, Chin. Phys. C **41**, 053107 (2017).
- [18] C. Tsallis, J. Statist. Phys. **52**, 479 (1988).
- [19] T.S. Biro, G. Purcsel, K. Urmosy, Eur. Phys. J. A **40**, 325 (2009).
- [20] T. Bhattacharyya, J. Cleymans, A. Khuntia, P. Pareek, R. Sahoo, Eur. Phys. J. A **52**, 30 (2016).
- [21] H. Zheng, L. Zhu, Adv. High Energy Phys. **2015**, 180491 (2015).
- [22] Z. Tang, Y. Xu, L. Ruan, G. van Buren, F. Wang, Z. Xu, Phys. Rev. C **79**, 051901 (2009).
- [23] B. De, Eur. Phys. J. A **50**, 138 (2014).
- [24] A. Adare et al. (PHENIX Collaboration), Phys. Rev. C **83**, 064903 (2011).
- [25] V. Khachatryan et al. (CMS Collaboration), JHEP **1105**, 064 (2011).
- [26] P.K. Khandai, P. Sett, P. Shukla, V. Singh, Int. J. Mod. Phys. A **28**, 1350066 (2013).
- [27] A. Adare et al. (PHENIX Collaboration), Phys. Rev. D **83**, 052004 (2011).
- [28] P. Sett, P. Shukla, Adv. High Energy Phys. **2014**, 896037 (2014).
- [29] P.K. Khandai, P. Sett, P. Shukla, V. Singh, J. Phys. G **41**, 025105 (2014).
- [30] K. Saraswat, P. Shukla, V. Kumar, V. Singh, Eur. Phys. J. A **53**, 5 (2017).
- [31] J. Cleymans, D. Worku, J. Phys. G **39**, 025006 (2012).
- [32] P. Sett, P. Shukla, Int. J. Mod. Phys. E **24**, 1550046 (2015).
- [33] Y-Q Gao, F-H Liu, Indian J. Phys. **90**, 319 (2016).
- [34] C. Tsallis, R.S. Mendes, A.R. Plastino, Physica A **261**, 534 (1998).
- [35] J. Cleymans, D. Worku, Eur. Phys. J. A **48**, 160 (2012).
- [36] J. Cleymans, M.D. Azmi, Eur. Phys. J. C **75**, 430 (2015).
- [37] J. Cleymans, M.D. Azmi, J. Phys. Conf. Ser. **668**, 012050 (2016).
- [38] B.C. Li, Z. Zhang, J.H. Kang, G.X. Zhang, F.H. Liu, Adv. High Energy Phys. **2015**, 741816 (2015).
- [39] P-Z Ning, L. Li, D-F Min, *Foundation of Nuclear Physics: Nucleons and Nuclei*, (Higher Education Press, Beijing, China, 2003).
- [40] C.D. Dermer, Astrophys. J. **280**, 328 (1984).

- [41] C-R Meng, *Chin. Phys. Lett.* **26**, 102501 (2009).
- [42] V. Khachatryan et al. (CMS Collaboration), *Phys. Lett. B* **768**, 103 (2017).
- [43] S. Chatrchyan et al. (CMS Collaboration), *Phys. Lett. B* **724**, 213 (2013).
- [44] J. Cleymans, G.I. Lykasov, A.S. Parvan, A.S. Sorin, O.V. Teryaev, D. Worku, *Phys. Lett. B* **723**, 351 (2013).
- [45] K. Aamodt et al. (ALICE Collaboration), *Phys. Lett. B* **696**, 328 (2011).
- [46] V.A. Okorokov, *Adv. High Energy Phys.* **2015**, 790646 (2015).
- [47] A. Bialas, W. Florkowski, K.Zalewski, *J. Phys. G* **42**, no. 4, 045001 (2015).
- [48] A.N. Makhlin, Yu.M. Sinyukov, *Z. Phys. C* **39**, 69 (1988).
- [49] D. Boal, C.G. Gelbke, B. Jennings, *Rev. Mod. Phys.* **62**, 553 (1990).
- [50] U. Mayer, E. Schnedermann, U. Heinz, *Phys. Lett. B* **294**, 69 (1992).
- [51] S.V. Akkelin, Yu.M. Sinyukov, *Phys. Lett. B* **356**, 525 (1995).
- [52] S. Chapman, P. Scotto, U. Heinz, *Phys. Rev. Lett.* **74**, 440 (1995).
- [53] P. Castorina, H. Satz, *Adv. High Energy Phys.* **2014**, 376982 (2014).
- [54] A.N. Tawfik, H. Yassin, E.R.A. Elyazeed, *Int. J. Mod. Phys. E* **26**, no. 03, 1750001 (2017).
- [55] H. Zhao, F-H Liu, *Adv. High Energy Phys.* **2014**, 742193 (2014).
- [56] C-Y Wong, G. Wilk, *Acta. Phys. Pol. B* **43**, 2047 (2012).
- [57] K. Urmosy, G.G. Barnafoldi, T.S. Biro, *Phys. Lett. B* **718**, 125 (2012).
- [58] G. Wilk, Z. Wldarczyk, *Eur. Phys. J. A* **48**, 161 (2012).
- [59] L. Marques, J. Cleymans, A. Deppman, *Phys. Rev. D* **91**, 054025 (2015).
- [60] L. Marques, E. Andrade-II, A. Deppman, *Phys. Rev. D* **87**, 114022 (2013).
- [61] M.D. Azmi, J. Cleymans, *J. Phys. G* **41**, 065001 (2014).



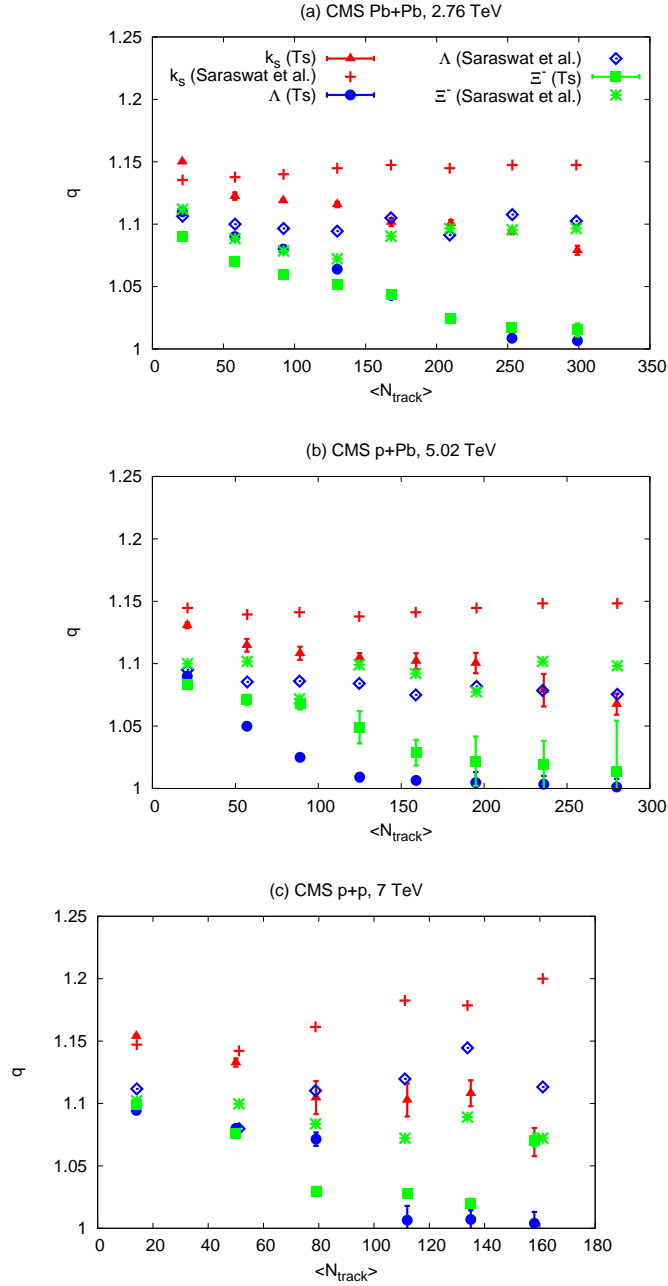


Fig. 4: (Color online) The fitting parameter  $q$  as a function of the event multiplicity  $\langle N_{\text{track}} \rangle$  for the strange particles  $K_s^0$ ,  $\Lambda$ , and  $\Xi^-$  which fitted using Tsallis and Boltzmann statistics for (a) Pb+Pb collision at  $\sqrt{s_{NN}} = 2.76$  TeV, (b) p+Pb collision at  $\sqrt{s_{NN}} = 5.02$  TeV, and (c) p+p collision at  $\sqrt{s_{NN}} = 7$  TeV.

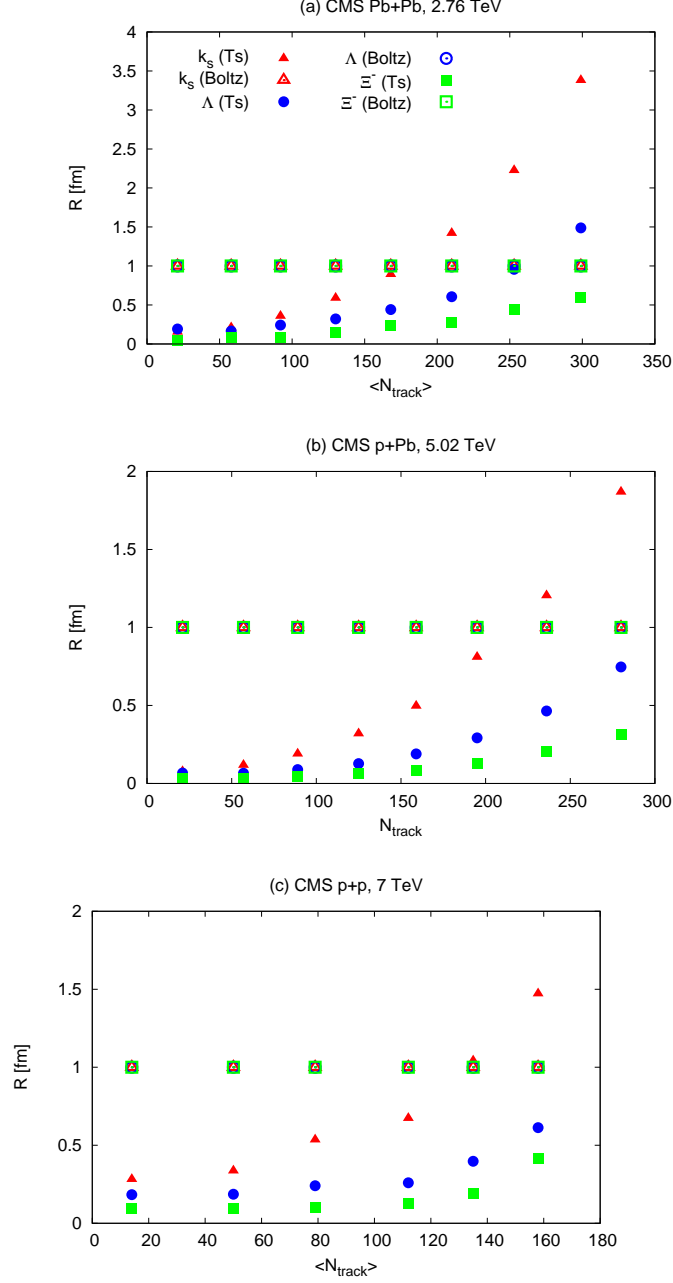


Fig. 5: (Color online) The fitting parameter  $R$  as a function of the event multiplicity  $\langle N_{\text{track}} \rangle$  for the strange particles  $K_s^0$ ,  $\Lambda$ , and  $\Xi^-$  which fitted using Tsallis and Boltzmann statistics for (a) Pb+Pb collision at  $\sqrt{s_{NN}} = 2.76$  TeV, (b) p+Pb collision at  $\sqrt{s_{NN}} = 5.02$  TeV, and (c) p+p collision at  $\sqrt{s_{NN}} = 7$  TeV.

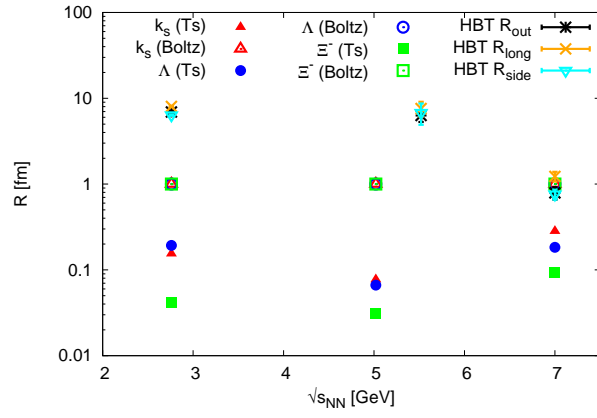


Fig. 6: (Color online) The parameter  $R$  as a function of the center-of-mass energies  $\sqrt{s_{NN}}$  for the obtained strange particles  $K_s^0$ ,  $\Lambda$ , and  $\Xi^-$  which fitted using Tsallis and Boltzmann statistics and values of HBT radii ( $R_{out}$ ,  $R_{long}$ ,  $R_{side}$ ) [45, 46, 47].

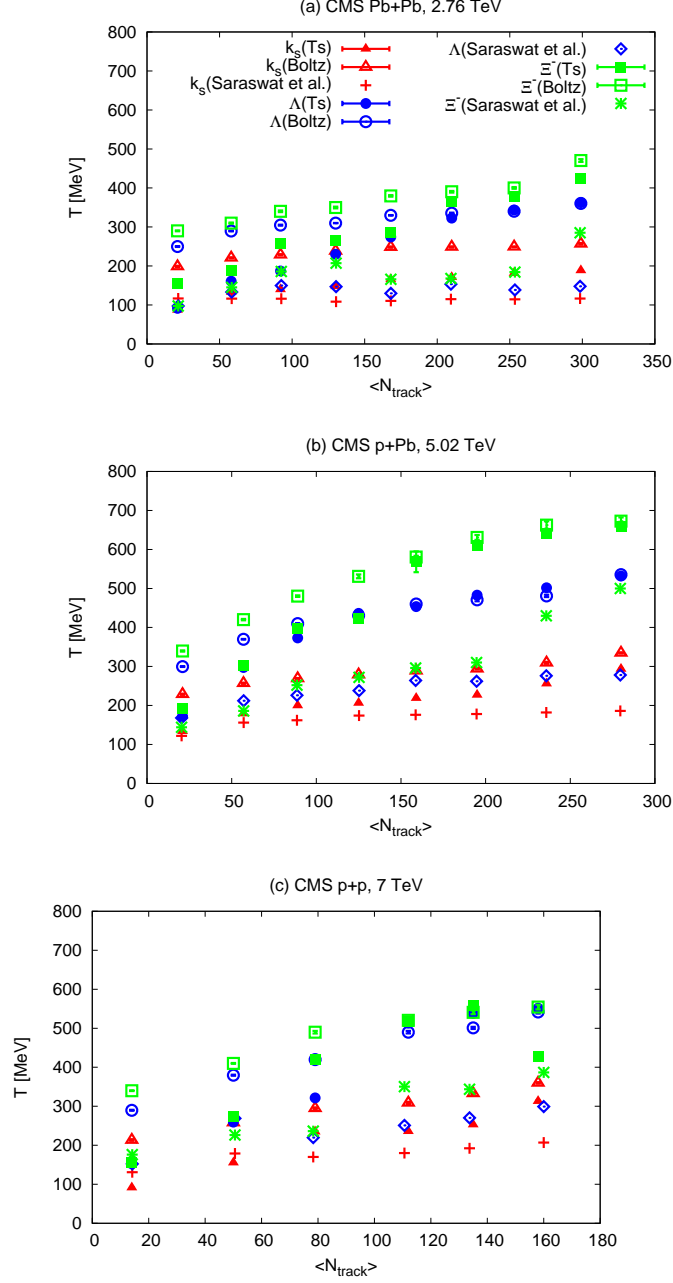


Fig. 7: (Color online) The fitting parameter  $T$  as a function of the event multiplicity  $\langle N_{\text{track}} \rangle$  for the strange particles  $K_s^0$ ,  $\Lambda$ , and  $\Xi^-$  which fitted using Tsallis and Boltzmann statistics- for (a) Pb+Pb collision at  $\sqrt{s_{NN}} = 2.76$  TeV, (b) p+Pb collision at  $\sqrt{s_{NN}} = 5.02$  TeV, and (c) p+p collision at  $\sqrt{s_{NN}} = 7$  TeV.

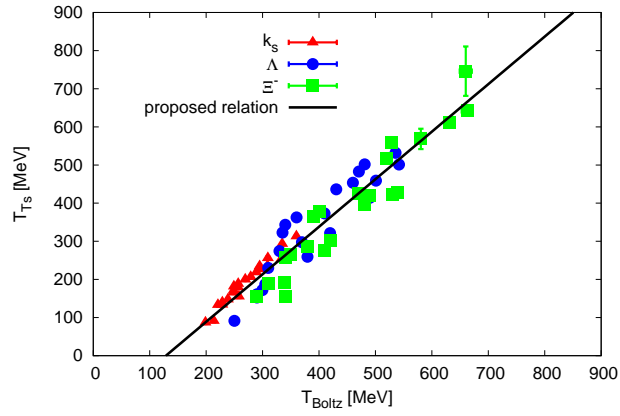


Fig. 8: (Color online) The Tsallis temperature  $T_{Ts}$  as a function of Boltzmann temperature  $T_{Boltz}$ . All values of temperatures obtained from Figs. 1, 2, and 3 which listed in Tables 1, 2, and 3 are given by symbols. The solid line represents the fitted result that given by Eq. 7.